Metabolic alkalinity release from large port facilities (Hamburg, Germany) and impact on coastal carbon storage

Mona Norbisrath[1,2], Johannes Pätsch[1,3], Kirstin Dähnke[1], Tina Sanders[1], Gesa Schulz[1,4], Justus E. E. van Beusekom[1], and Helmuth Thomas[1,2]

[1]Institute of Carbon Cycles, Helmholtz-Zentrum Hereon, Geesthacht, 21502, Germany
[2]Institute for Chemistry and Biology of the Marine Environment, Carl von Ossietzky University Oldenburg, Oldenburg, 26129, Germany
[3]Institute of Oceanography, University Hamburg, Hamburg, 20146, Germany
[4]Institute of Geology, Center for Earth System Research and Sustainability (CEN), University Hamburg, Hamburg, 20146, Germany

Correspondence to: Mona Norbisrath (mona.norbisrath@gmail.com)

Abstract

Metabolic activities in estuaries, especially these of large rivers, profoundly affect the downstream coastal biogeochemistry. Here, we unravel the impacts of large industrial port facilities, showing that elevated metabolic activity in the Hamburg port (Germany) increases total alkalinity (TA) and dissolved inorganic carbon (DIC) runoff to the North Sea. We explained this activity to be fueled by the imports of particulate inorganic carbon, particulate organic carbon, and particulate organic nitrogen (PIC, POC, and PON) from the upstream Elbe River resulting in a maximum TA generation of 90 %, TA generation due to $CaCO_3$ dissolution in the entire estuary. The remaining 10 % of TA generation can be attributed to anaerobic metabolic processes such as denitrification of remineralized PON, or other pathways. The Elbe Estuary as a whole adds approximately 15 % to the overall DIC and TA runoff. Both the magnitude and partitioning among these processes appear to be sensitive to climatic and anthropogenic changes. Thus, with increased TA loads, the coastal ocean (in particular) would act as a stronger CO_2 sink, resulting in changes to the overall coastal systems capacity to store CO_2.

1 Introduction

Anthropogenic activities have increased nutrient and organic matter (OM) fluxes to the coastal ocean e.g. (Howarth et al., 1996). Capable of retaining part of the nitrogen flux through denitrification pathways, estuaries play an important role as regulators of the coastal ocean system (Frankignoulle et al., 1998;Howarth et al., 2011;Seitzinger, 1988;Smith and Hollibaugh, 1993). With intense biogeochemical cycling typically, estuaries can be divided geographically; the outer estuary acts as a sink of CO_2, while the inner estuary often acts as a source (Borges et al., 2006;Cai and Wang, 1998;Frankignoulle et al., 1998). Deep estuaries and semi-enclosed seas, such as the Gulf of St. Lawrence or the Baltic Sea, are mostly permanently stratified. This means that they have a strong memory effect due to ventilation time scales of the subsurface waters that are beyond the

annual scale. Due to the long ventilation time, these waterbodies have a high storage capacity for carbon species such as DIC and nutrients e.g. phosphorus, and may hold oxygen deficits (Gilbert et al., 2005;Mucci et al., 2011) leading to high N retention (De Jonge et al., 1994). Contrasting deep estuaries, shallow ones like the Elbe Estuary, are usually well ventilated (Abril et al., 2002;Pein et al., 2021). This enables them have a strong benthic-pelagic coupling due to vertical exchange, which causes direct

35 respond within these areas to seasonal forcing.

~~The Elbe Estuary is located in the northern part of Germany and is about 140 km long. It encompassing an area that begins at the weir in Geesthacht (Elbe stream km 586), crosses the port of Hamburg (Elbe stream km 623) and discharges near Cuxhaven (Elbe stream km 727) into the North Sea, a semi-enclosed shelf sea of the eastern North Atlantic (Fig. 1). The North Sea influences the estuary with its strong tidal cycles, resulting in a semi-diurnal tidal range of 3.6 m in the port of Hamburg~~

40 ~~(Amann et al., 2012), the third largest port in Europe, and provides a continuous exchange of fresh and marine water.~~

The increased flux of organic matter (OM) during eutrophication (e.g. from agricultural fertilizers and wastewater) can ~~cause~~ generate ~~large~~ phytoplankton blooms in both ~~in~~ rivers and ~~in~~ the coastal zone (Hardenbicker et al., 2016;Van Beusekom et al., 2019). This can lead to higher rates of ~~Whose decay increases~~ oxygen consumption (Schöl et al., 2014;Spieckermann et al., 2021), which can drive hypoxia in stratified bodies of water, such as ~~and may lead to declining oxygen levels in bottom water,~~

45 ~~and possibly hypoxia in~~ estuaries and the coastal ocean ~~zones~~ (Frankignoulle et al., 1996;Gilbert et al., 2005;Große et al., 2016;Howarth et al., 2011;Mucci et al., 2011;Nixon, 1995;Rabalais et al., 2002, 2001;Thomas et al., 2009). A hotspot of organic matter turnover exists in, and downstream the Hamburg port (Pein et al., 2021;Sanders et al., 2018;Schöl et al., 2014). ~~Just upstream of the port of Hamburg,~~ where dredging activities have increased the depth from around 5 m (upstream the port)

to about 20 m to guarantee accessibility of large seagoing vessels. By increasing the depths, seasonal stratification in the

50 Hamburg port is favored, resulting in the formation of oxygen-poor or even hypoxic sedimental zones (Kerner, 2007;Pein et al., 2021). These sediment structures are essential for anaerobic metabolic processes that use terminal electron acceptors other than O_2 (e.g. NO_3^-, Fe^{3+}, Mn^{4+}, SO_4^{2-}) to respire organic matter, which are of particular interest as they release alkalinity in varying stoichiometry (Brewer and Goldman, 1976;Chen and Wang, 1999;Hu and Cai, 2011;Wolf-Gladrow et al., 2007). The resulting reduced products (e.g. N_2, H_2S, Fe^{2+}) can be transported back into the water column, but if the reduced products, with

55 the exception of N_2, can be reoxidized in the water column, any increase in alkalinity from the generation will be consumed. The reduced products can escape two ways: (I) reoxidation via permanent burial (e.g. FeS_2 (pyrite)), or (II) via escape to the atmosphere (e.g. N_2). In addition to anaerobic processes, dissolution of calcium carbonate ($CaCO_3$) also generates alkalinity in a TA:DIC ratio of 2:1, which can be reversed by precipitation (Chen and Wang, 1999). Earlier studies (Francescangeli et al., 2021;Kempe, 1982) state that the hydro-chemical conditions favoring $CaCO_3$ dissolution in the lower Elbe Estuary. Thus,

60 for the purpose of this paper, we consider $CaCO_3$ dissolution as a metabolic process favored by lower pH, e.g. bacterial degradation of organic matter, leading to generation of alkalinity.

By combining observational and modeling techniques (Schwichtenberg et al., 2020), this study sheds light on the biogeochemical cycling of TA, DIC and in particular nitrate. From this, this study aims to answer the questions: a) how much

metabolic alkalinity is released from the Elbe Estuary into downstream coastal waters of the North Sea, and b) how the North

65 Seas CO_2 uptake changes under altered metabolic alkalinity inputs as a consequence of climatic and anthropogenic changes.

2 Methods

2.1 Study site

Located in the norther part of Germany, the Elbe Estuary extends approximately 140 km (Fig. 1), encompasses an area that begins at the weir in Geesthacht (Elbe stream km 586), crosses the port of Hamburg (Elbe stream km 623), and discharges

70 near Cuxhaven (Elbe stream km 727) into the North Sea. The North Sea is a semi-enclosed shelf sea of the eastern North Atlantic that influences the estuary with its strong tidal cycles. This results in a semi-diurnal tidal range of 3.6 m in the port of Hamburg (Amann et al., 2012), the third largest port in Europe, and provides a continuous exchange of fresh and marine water. The Elbe has an average annual long-term discharge of 704 m^3 sec^{-1}, measured at the last tide-free long term sampling station in Neu Darchau (Elbe stream km 536) (Amann et al., 2012). Water depth in the Elbe Estuary is around 15-20 m but sharply

75 decreased to 5 m upstream Elbe stream km 620 (Hamburg port). For mass balance calculations, we separated the Elbe Estuary in 6 boxes, indicated by the lines in Fig. 1, of which box 1 (upstream the Hamburg port) and box 6 (North Sea) act as boundary conditions.
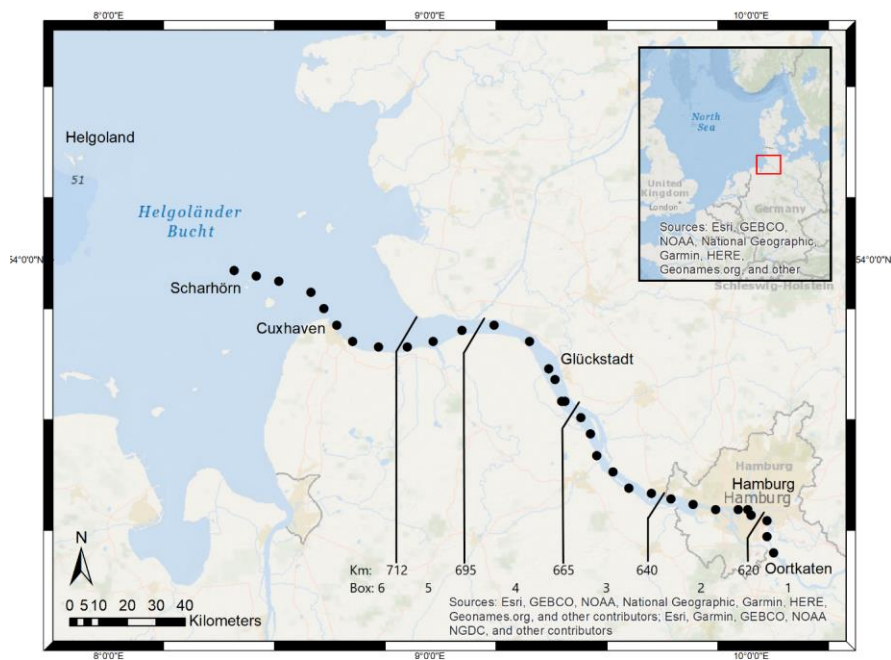
Figure 1. Study site. The Elbe Estuary with sampling stations in June 2019 (dots) and the spatial separation of the estuary for the mass balance calculation (lines), whereby box 2 indicates the port of Hamburg in the upper estuary, box 3 and box 4 in the middle estuary, and box 5 in the lower estuary.

2.2 Sampling

This study is based on samples that we collected during a cruise (LP20190603) on RV *Ludwig Prandtl* on two consecutive days in June 2019 during ebb tide. We sampled from the German Bight around the island of Scharhörn upstream to Oortkaten situated in the riverine part of the estuary (Fig. 1). Discrete surface water (1.2 m depth) samples were collected every 20 minutes from out of a bypass of the flow-through FerryBox system (Petersen et al., 2011). Concurrently, the FerryBox provideds the required physical parameters such as salinity, temperature and oxygen. Water depth in the Elbe Estuary was around 15-20 m but sharply decreased to 5 m upstream Elbe stream km 620. For mass balance calculations, we separated the Elbe Estuary in 6 boxes, indicated by the lines in Fig. 1, of which box 1 (upstream the Hamburg port) and box 6 (North Sea) act as boundary conditions.

First, water samples for total alkalinity (TA) and dissolved inorganic carbon (DIC) measurements were filled into 300 mL BOD (biological oxygen demand) bottles and preserved with 300 µL saturated mercury chloride ($HgCl_2$) to stop biological activity. The bottles, which are free of air bubbles, were then sealed with ground-glass stoppers coated in Apiezon® type M grease, and protected against opening by plastic caps. Samples were stored in a cool place in the dark until measured.

Samples for nutrients and stable isotopes of nitrate (NO_3^-) were collected to measure the concentration and the isotopic composition of nitrate respectively. We collected three 15 mL Falcon tubes for triplicate nutrient measurements, and one 100 mL PE bottle (acid-washed overnight with 10 % HCl) for stable isotope analysis. Samples were filtered through pre-combusted GF/F filters, and then frozen for onshore analyses.

We used pre-combusted (4 h, 450 °C) GF/F filters to sample for particulate inorganic carbon (PIC) and particulate organic carbon and nitrogen (POC, PON) concentrations that we stored frozen until onshore analysis.

2.3 Analytical procedures

2.3.1 TA and DIC

First, water samples for total alkalinity (TA) and dissolved inorganic carbon (DIC) measurements were filled in 300 mL BOD (biological oxygen demand) bottles and preserved with 300 µL saturated mercuric chloride ($HgCl_2$) to stop biological activity. We sealed the bottles with ground-glass stoppers, Apiezon® type M grease, free of air bubbles and protected them against opening with plastic caps. Samples were stored in a cool place in the dark until measured.

We performed the TA and DIC measurements at Helmholtz-Zentrum Hereon using a VINDTA 3C (Versatile INstrument for the Determination of Total dissolved inorganic carbon and Alkalinity, marianda - marine analytics and data). VINDTA 3C measures TA by potentiometric titration and DIC by coulometric titration (Shadwick et al., 2011). We used Certified Reference Material (CRM batch # 187) provided by A. G. Dickson (Scripps Institution of Oceanography) to calibrate TA and DIC measurements and ensured a precision of $\pm$ 2 µmol kg^{-1}.

2.3.2 Nutrients and stable nitrate isotopes

Samples for nutrients and stable isotopes of nitrate (NO_3^-) were collected concurrently with TA and DIC samples, to measure the concentration and the isotopic composition of nitrate respectively. We collected three 15 mL Falcon tubes for triplicate nutrient measurements, and one 100 mL PE bottle (acid-washed overnight with 10 % HCl) for stable isotope analysis. Samples were filtered through pre-combusted GF/F filters, and then frozen for onshore analyses.

In order to determine nutrients, we used a continuous flow automated nutrient analyzer (AA3, SEAL Analytical) with a standard colorimetric technique (Hansen and Koroleff, 2007) to measure concentrations of dissolved nitrate (NO_3^-), nitrite (NO_2^-) and phosphate (PO_4^{3-}). In order to measure ammonium (NH_4^+), we used a fluorometric method (Kérouel and Aminot, 1997). All samples were measured in triplicate.

We applied the denitrifier method (Casciotti et al., 2002;Sigman et al., 2001) to determine the stable isotope ratios of $\delta^{15}N$ and $\delta^{18}O$ of nitrate. By using denitrifying *Pseudomonas aureofaciens* (ATCC#13985), which lacks nitrous oxide reductase activity to reduce nitrate and nitrite in the filtered water sample to nitrous oxide (N_2O), we were able to measure the produced N_2O by a GasBench II coupled to an isotope mass spectrometer (Delta Plus XP, Fisher Scientific). Concurrently, we used two

125 international standards (USGS34, $\delta^{15}N\text{-}NO_3^- = -1.8$ ‰, $\delta^{18}O\text{-}NO_3^- = -27.9$ ‰; IAEA, $\delta^{15}N\text{-}NO_3^- = +4.7$ ‰, $\delta^{18}O\text{-}NO_3^- = +25.6$ ‰), and one internal standard ($\delta^{15}N\text{-}NO_3^- = +7.6$ ‰, $\delta^{18}O\text{-}NO_3^- = +24.4$ ‰) for data correction in each run. The standard deviation for standards and samples was <0.2 ‰ (n = 4) for $\delta^{15}N\text{-}NO_3^-$ and <0.5 ‰ (n = 4) $\delta^{18}O\text{-}NO_3^-$. The nitrite concentration of the samples was usually less than 5 %, but when it exceeded this threshold, nitrite in the samples was removed with Sulfamic Acid (4 % Sulfamic Acid in 10 % HCl) prior to analysis (Granger and Sigman, 2009).

130 Variations in the natural abundance of stable isotopes are represented as relative differences in isotope ratios. The isotope ratio R, is the ratio of heavy to light isotopes. Since isotope differences are very small, the delta-δ-notation is used to describe the isotopic composition of samples (Eq. 1). Therefore, the isotopic ratio of a sample (R_{sample}) is given relative to the ratio of an internationally accepted reference material ($R_{reference}$). For this study, atmospheric N_2 and Vienna Standard Mean Ocean Water (VSMOW) are the reference materials for nitrogen and oxygen, respectively. The delta-δ-notation is calculated as follows:

135 $$\delta\ (‰) = \left(\frac{R_{sample} - R_{reference}}{R_{reference}}\right) \times 1000 \tag{1}$$

We identified the nitrate sources river upstream from the minimum isotope values at Elbe stream km 705 using Eq. 2. Here, we focused on the upper fresh water part of the estuary to identify the isotope values and the source of the additional nitrate (δ_{ad}) added to the estuary between Elbe stream km 609 and 705. To investigate this further, we employed a simple mixing model (Sanders et al., 2018) with the $\delta^{15}N$ and $\delta^{18}O$ values and associated nitrate concentrations (C):

140 $$\delta_{ad} = \frac{((\delta_{705}\ x\ C_{705}) - (\delta_{609}\ x\ C_{609}))}{(C_{705} - C_{609})} \tag{2}$$

2.3.3 Ancillary parameters

~~We used pre-combusted (4 h, 450 °C) GF/F filters to sample for particulate organic carbon (POC) and particulate organic nitrogen (PON) concentrations.~~ In order to determine POC and PON, ~~First,~~ the filters were measured for total carbon (TC) as a bulk sample first. Then, the filters were acidified 3 times with 1 N HCl and measured again for POC. The particulate inorganic

145 carbon (PIC) was derived from the difference in C content of the unacidified and acidified filters (TC-POC). The filters were measured with a CHN-elemental analyzer (Eurovector EA 3000, HEKAtech GmbH) in the Institute of Geology, University Hamburg, where the measurements were calibrated against the standards Sulfanilamide (C = 41.84 %, N = 16.27 %) und Acetanilide (C = 71.09 %, N = 10.36 %).

We directly measured the oxygen content with the FerryBox O_2 optode (Optode 3830, Aanderraa Instruments AS,

150 Norway)(Petersen et al., 2011), and calibrated it with reference to parallel samples analyzed using the Winkler method.

The water depths that we used for the mass balances (see below) were measured during the cruise with the on board Acoustic Doppler Current Profiler (WorkHorse Broadband ADCP 1200kHz, Firmware Version 51.40.) (Cysewski et al., 2018).

2.4 Gas flux calculation

As an input function for the mass balances (see below), we estimated CO_2 and O_2 gas exchange (F) between the atmosphere
155 and water. We used the following equation:

$$F_{gas} = k_{gas} \; x \; (d_{gas}) \tag{3}$$

where k_{gas} is the transfer velocity of the gases (O_2 and CO_2), and d_{gas} is the difference between the atmospheric and aquatic
concentration, calculated as follows:

$$d_{gas} = [gas]_{at\;100\%\;saturation} - [gas]_{observed} \tag{4}$$

160 The CO_2 concentration of the sample (observed) was computed from DIC, TA, salinity and temperature using the CO_2SYS
program by Lewis and Wallace (1998), and the dissociation constants for fresh water by Millero (1979). The CO_2 concentration
of the sample corresponds the mentioned pCO_2. The CO_2 concentration (at 100 % saturation) was obtained from TA and the
global atmospheric CO_2 saturation of 416 ± 0.13 µatm (Dlugokencky and Tans, 2021) by using the same previously mentioned
program and constants.

165 We calculated the transfer velocity after Wanninkhof (2014) as follows:

$$k_{gas} = \frac{0.251 \; x \; (U_{10})^2}{(\frac{Sc}{Sc_{ref}})^{-0.5}} \tag{5}$$

where 0.251 is the coefficient of gas transfer; U_{10} is the wind speed in m sec $^{-1}$ measured in situ at 10 m height by the federal
authority "Deutscher Wetterdienst" (DWD) (provided by DWD (2020); Sc is the Schmidt number, the kinematic viscosity of
water divided by the diffusion coefficient of the gas (Wanninkhof, 2014); and Sc_{ref} is the Sc value relative to the reference
170 conditions of the gas at 20 °C in fresh water, which is 510 for O_2 and 600 for CO_2. The uncertainty of the flux calculation has
been estimated to 20 % (Wanninkhof, 2014;Watson et al., 2009).

2.5 Mass balances

2.5.1 Box model approach

Based on our observations, we used a box model approach to balance the net dissolved budgets of TA, DIC, NO_3^- and O_2 in
175 the Elbe Estuary (Fig. 2). The box model approach allowed us to distinguish the conservative contributions from the marine
and fresh water end-members based on salinity (i. e. baseline), the input and output values as advected transport, and the
atmospheric gas exchange (O_2 and CO_2), of the observed parameters TA, DIC, NO_3^- and O_2 between and within boxes. The
resulting differences are the closing terms given as net dissolved budgets, and referred to here as metabolic gains. To attribute
the potential processes affecting metabolic generation; we distinguished between pelagic generation, which is associated with
180 aerobic conditions, i.e. nitrification, which consumes TA, and benthic generation, which corresponds to anaerobic conditions,
where anaerobic metabolic processes generate TA. We defined 6 boxes based on spatial and salinity considerations, with box
1 representing the fresh water (upstream the Hamburg port) and box 6 the coastal ocean (North Sea) (Table 1). Both boxes, 1
and 6 determined the start and end, were not balanced, and acted as boundary conditions. Calculation and end-member

properties are shown in Table 1. Discharge per box was calculated using the observed depths, in combination with an average river discharge value (provided by FGG (2021)) measured from the last tide-free at the long term monitoring station Neu Darchau (Elbe stream km 536). Accordingly, we computed the fill time, or in other words, the fresh water flushing time of each box, as box volume divided by discharge (Table 1).

We used the following equation to calculate the metabolic gains by assuming a steady state:

$$\frac{\delta c}{\delta t} = 0 = F_{\text{Input}} + F_{\text{Output}} + F_{\text{Baseline}} + F_{\text{ASF (O2,CO2)}} + F_{\text{Metabolic}} \qquad (6)$$

where F_{Input} is the input value, F_{Output} the output value, F_{Baseline} the salinity corrected baseline value, $F_{\text{ASF (O2, CO2)}}$ the air-sea flux of O_2 and CO_2, respectively, and $F_{\text{Metabolic}}$ the metabolic gain as the closing term.
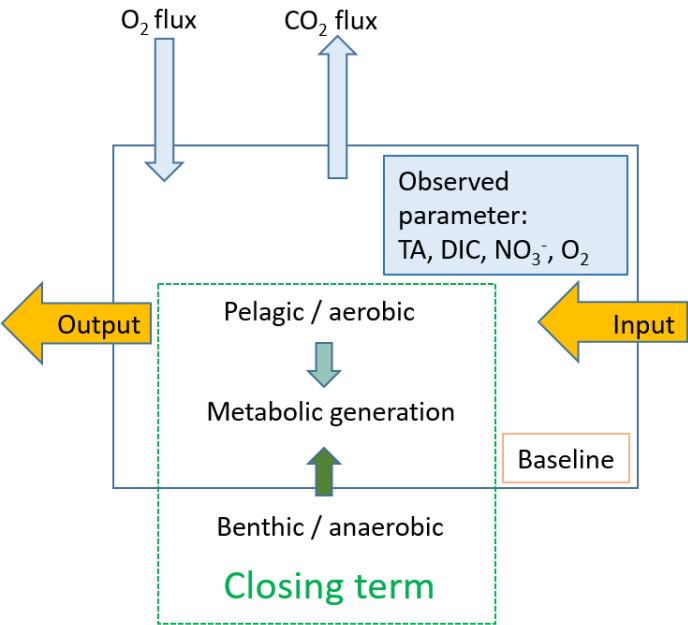
Figure 2. Schematic mass balance approach. We used a box model to balance the net dissolved budgets along the Elbe Estuary. The observed parameters are shown in light blue, the closing term is set as metabolic generation (green), which is fueled by pelagic, i.e. aerobic, and benthic, i.e. anaerobic processes, but without allocating how much of what is generated where. The input and output is shown in yellow, and the latter acts as the input for the downstream box. To complete DIC and O2, we included the atmospheric gas exchange. The baseline is calculated assuming conservative mixing of fresh and marine end-members.

Table 1. Elbe Estuary data for the mass balance calculation. The water depths were from an Acoustic Doppler Current Profiler (ADCP) on board of RV *Ludwig Prandtl*, and the river length is based on the Elbe stream km. The river width is based on measurements with Google Maps®, while a standardized river width of 2 km was used for box 3, 4 & 5. The average river discharge on our sampling days was 423 m^3 sec^{-1} (provided by FGG (2021)) measured at the last tide-free long term sampling station in Neu Darchau (Elbe stream km 536). Average box values are given for total alkalinity (TA), dissolved inorganic carbon (DIC), nitrate (NO$_3^-$) and salinity. For the outer boundary conditions (box 6), we used a maximum salinity of 33.26, and respective TA (2449 µmol kg^{-1}), DIC (2132 µmol kg^{-1}), and NO$_3^-$ (0.1 µmol L^{-1}) values taken on cruise HE541 (54.062456° N, 8.015919° E), which took place two months later in September 2019 and represents average summer time values for the German Bight. Standard deviation ± sd as spatial variability is given when possible.

Species	Unit	Box 1	Box 2	Box 3	Box 4	Box 5	Box 6
Elbe stream km	km	607 - 619	619 - 639	639 - 666	666 - 693	693 - 710	-
Stream with	km	0.3	0.5	2.0	2.0	2.0	-
Stream length	km	12	20	27	27	17	-
Depth	km	0.00493	0.01392	0.016056	0.011999	0.016926	-
Water volume	km^3	0.0177	0.1392	0.8670	0.6479	0.5755	-
Fill time	d	0.4865	3.8094	23.7241	17.7304	15.7468	-
av. TA ± sd	µmol kg^{-1}	1289 ± 8	1512 ± 40	1630 ± 42	1733 ± 35	1879 ± 21	2449
av. DIC ± sd	µmol kg^{-1}	1288 ± 30	1589 ± 58	1701 ± 39	1793 ± 29	1896 ± 4	2132
av. NO$_3^-$ ± sd	µmol L^{-1}	74 ± 0	91 ± 6	114 ± 7	139 ± 9	161 ± 6	0.1
av. Salinity ± sd	-	0.41 ± 0.0	0.45 ± 0.0	0.61 ± 0.1	1.07 ± 0.4	5.17 ± 1.4	33.26

The uncertainty of the closing term has been estimated by using the analytical measurement precision of 2 µmol kg^{-1} for DIC and TA, 0.5 µmol L^{-1} for NO$_3^-$, and 5 % for O$_2$ (Petersen et al., 2011). The gas exchange was considered with an uncertainty of 20 % (Wanninkhof, 2014;Watson et al., 2009). The river discharge uncertainty was 5 % (Léonard et al., 2000) and was added to the error in the end. The analytical measurement precision of POC and PON was 0.05 % and 0.005 %, respectively (Gaye et al., 2022), calculated from the average box 1 values. We calculated the analytical errors with the following equation per parameter and box:

$$X = (\textstyle\sum_i x_i^2)^{0.5} \tag{7}$$

where X is the combined error and x_i are the errors of the individual observations.

2.5.2 TA source attribution

In order to assess the ~~total alkalinity~~TA gains throughout Elbe Estuary, we compared the mass balance gains with the measured riverine POM properties. Therefore, we used the riverine PIC and POC concentrations that were imported to the Hamburg port, where they can be converted in DIC and other molecules due to various processes. PIC mainly consists CaCO$_3$. Depending on the ambient saturation, it is converted into DIC and Ca^{2+} by dissolution or vice versa by precipitation.

By using the imported riverine PIC and POC, we derived the maximum amount TA fueled by CaCO₃ dissolution as source, and estimated the remaining amount of PIC transported downstream.

In order to estimate the TA gain that can be fueled by CaCO$_3$ dissolution, we considered the observed metabolic DIC, the average imported PIC:TC (particulate inorganic carbon:total carbon) ratio (0.29 ± 0.05), and the TA:DIC ratio for CaCO$_3$
225   dissolution (2) (Chen and Wang, 1999). To get the remaining DIC generated by e.g. organic matter respiration (POC), we multiplied the metabolic DIC gain by 0.71 ($1 - 0.29 = 0.71$). To arrive at the corresponding TA that was not fueled by CaCO$_3$ dissolution, we subtracted the TA fueled by CaCO$_3$ dissolution from the entire metabolic TA gain. We performed all calculations per box.

To estimate the amount of PIC that is transported through the estuary, but not used for TA generation by CaCO$_3$ dissolution,
230   we used the imported PIC (multiplied by the ratio of 2) and subtracted the previously calculated corresponding TA. The following boxes then do not refer to the imported PIC, but to the product of the previous box that correspond to the unused transported PIC. In case of negative values such as in box 4, we set the transported PIC in the following calculation to 0.

For the coupling of carbon and nitrogen, we used the imported PON to estimate the amount that is transported, unused, through the Elbe Estuary, and to estimate whether or not riverine PON import is sufficient to generate NO$_3^-$ and TA.
235   For estimating the TA generation fueled by denitrification (that we attribute here to imported riverine PON), we calculated the amount of PON that is available for denitrification by subtracting the nitrified PON (i.e. entire estuarine metabolic NO$_3^-$ gain) of the imported PON (box 1). With the calculated PON available for denitrification, the ratio of TA:DIC resulting from denitrification (0.9) (Chen and Wang, 1999), and the entire TA gain that is not fueled by PIC, we calculated the possible TA gain from PON that could be generated in the estuary without the occurrence of nitrification.

240   To estimate the amount of PON that can be transported downstream, we used the imported PON, the sum of the NO$_3^-$ gain of the mass balances, the previously calculated TA gain that was not fueled by PIC, and the TA:DIC ratio (0.9) for denitrification. The following boxes then do not refer to the imported PON, but to the product of the previous box. In case of negative values such as in box 4, we set the transported PON in the following calculation to 0.

2.6 Biogeochemical simulations

245   For estimating the effects of metabolic produced alkalinity in the estuary on the North Sea and the continental shelf, we applied the 3D-ECOHAM model (Schwichtenberg et al., 2020). Pätsch and Kühn (2008) first described the ECOHAM model domain for this study (see their Fig. 1). Meteorological forcing for both models was derived from the ERA5 reanalysis dataset (Hersbach et al., 2020).

The physical parameters temperature, salinity, horizontal and vertical advection, as well as turbulent mixing were calculated
250   using the hydrodynamic model HAMSOM (Backhaus, 1985). This is a baroclinic primitive equation model using the hydrostatic and Boussinesq approximations. Details are described by Backhaus and Hainbucher (1987) and Pohlmann (1996). We ran the hydrodynamic model prior to the biogeochemical part. We saved the daily result fields and ran the biogeochemical model in offline mode.

The relevant biogeochemical processes and their parameterizations have been detailed in Lorkowski et al. (2012). TA and DIC are computed prognostically. The pelagic biogeochemical part is driven by planktonic production and respiration, calcite formation and dissolution, pelagic and benthic degradation and remineralization, and also by atmospheric deposition of reactive nitrogen. All of these processes affect TA. The air-sea flux of CO_2 was calculated for the North Sea region between 51° N and 59.5° N according to (Wanninkhof, 2014).

We extracted the year 2001 from the simulation run 1979-2014 for the analysis in this paper. Four different scenarios (50, 86, 100, and 150 % TA load) were run, with the 100 % scenario being the reference scenario with full riverine TA and DIC input. In comparison, the 86 % scenario reflects river input without the metabolic alkalinity generation corresponding to our calculated metabolic TA generation of 14 % throughout the Elbe Estuary. We ran two other scenarios, one with a reduced TA load (50 %) and one with an increased TA load (150 %) for a broader comparison. We used daily data of fresh water fluxes from 254 rivers discharging into the North Sea (Große et al., 2017). We applied corresponding river load data of nutrients, organic matter, DIC, and TA.

3 Results and Discussion

3.1 Salinity, TA, DIC, and nutrient distribution along the estuary

Along the Elbe Estuary transect, the salinity varied from 0.40 in the fresh water part (Elbe stream km 609-680), to 27.84 in marine waters in the German Bight. The strongest salinity gradient was observed between Elbe stream km 683 and 715 (box 5, tidal front) with an increase of 10 (Fig. 3a). The limited influence of salinity in the fresh water part, visible in Fig. 3a, limited the clear subdivision of the boxes 1 to 3 in Fig. 3b.

TA and DIC increased from the upper estuary (Elbe stream km 609) to the mouth of the estuary (Fig. 3a), where the lowest concentrations were found in Oortkaten (1281 µmol TA kg^{-1} and 1256 µmol DIC kg^{-1} at 0.41 salinity), and the highest were found around Scharhörn (2272 µmol TA kg^{-1} and 2016 µmol DIC kg^{-1} at 27.84 salinity). In marine and brackish waters of the Elbe Estuary, TA was higher than DIC, while in the fresh water part of the estuary, DIC was higher than TA. At a salinity of 6.96, TA and DIC were equal with 1922 µmol kg^{-1}. The strongest increase in TA was observed in the fresh water part, between Elbe stream km 609 and km 670 (Fig. 3a). While in the outer estuary, TA and DIC increased almost proportional to the salinity gradient without obvious biological impact (Fig. 3a,b).

Nitrate (NO_3^-) concentrations increased from 73 µmol NO_3^- L^{-1} near Oortkaten to a maximum of 165 µmol NO_3^- L^{-1} in the lower estuary at a salinity of 5.08 (Elbe stream km 705, box 5) (Fig. 3a), which is downstream of the maximum turbidity zone (MTZ is located between Elbe stream km 664-670, not shown). Further downstream, nitrate mixed conservatively with low NO_3^- seawater to 15 µmol NO_3^- L^{-1} at km 750.

Ammonium (NH_4^+) reached a pronounced maximum of 15 µmol NH_4^+ L^{-1} in the Hamburg port area, located upstream of the NO_3^- maximum, while varying in a range around 1 µmol NH_4^+ L^{-1} in the remainder of the estuary (Fig. 3a). This maximum

coincides with the strongest gradients in DIC and TA and can be attributed to high remineralization rates in the port area, as is also evident by the high apparent oxygen utilization (AOU) (Fig. 3a).

Phosphate (PO_4^{3-}) trends are comparable to nitrate, where a sharp increase in concentration is seen in the Hamburg port area, and a maximum concentration of 2 µmol PO_4^{3-} L^{-1} in the lower estuary (box 5), coinciding with the TA and DIC trend.

The $\delta^{15}N$-NO_3^- and $\delta^{18}O$-NO_3^- isotopic values were found to be higher in the upper estuary, and decreased downstream to their respective minima at km 705, coinciding with the NO_3^- maximum. In the fresh water part, the $\delta^{15}N$ and $\delta^{18}O$ values ranged from 12.4 ‰ to 17.1 ‰, and from 5.1 ‰ to 9.1 ‰, respectively.

The $\delta^{15}N$ values of suspended particulate matter (SPM) ($\delta^{15}N_p$) showed a pronounced increase from 6 to 10 ‰ in box 2, indicating an enrichment of heavy isotopes in the particulate matter due to the degradation of particulate organic matter (POM). This strong increase coincides with the ammonium peak and the declining $\delta^{15}N$-NO_3^-.
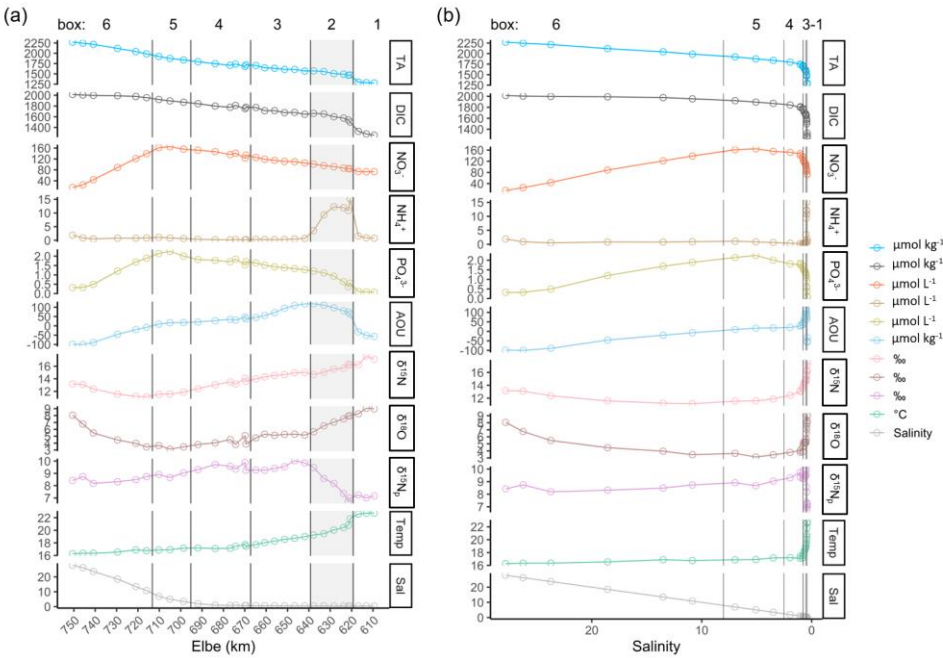
Figure 3. Spatial and salinity dependent observed parameter distribution along the Elbe Estuary. The data are from two days in June 2019. (a) Spatial observed parameter distribution from the inner estuary (Elbe stream km 609, right side) to the German Bight around the island of Scharhörn (computed Elbe stream km 750, left side). Total alkalinity (TA), dissolved inorganic carbon (DIC), nitrate (NO_3^-), ammonium (NH_4^+), phosphate (PO_4^{3-}), apparent oxygen utilization (AOU), delta values of nitrate isotopes ($\delta^{15}N$, $\delta^{18}O$) of filtered water, and

300 of suspended particulate matter ($\delta^{15}N_P$), as well as temperature (Temp) in ° C, and salinity (Sal) are shown. The vertical lines indicate the designated boxes for the mass balance calculation, in which the inner boundary (box 1) is on the right side of the plot, followed by the shaded box 2 with the Hamburg port area (upper estuary), boxes 3 and 4 (middle estuary), 5 (lower estuary), and the outer, marine boundary (box 6) on the left side of the plot. (b) Salinity dependent observed parameter distribution. Note the different y-axis scales within the different panels of both plots.

305 **3.2 Metabolic activity in the port**

The North Sea's carbonate system is affected by the surrounding coastal areas (Schwichtenberg et al., 2020), necessitating a specific investigation of estuarine based TA generation and an estimation of its impact on the oceanic CO_2 uptake capacity. In order to determine the TA, DIC, and O_2 related metabolic activity in the Elbe Estuary, we estimated the air-sea gas exchange of CO_2 and O_2 as these are non-advective processes along the Elbe Estuary (Fig. 4a, Table 2). Upstream of the port of Hamburg,

310 the pCO_2 was slightly supersaturated (465 µatm) relative to the atmosphere (416 µatm). Within the Hamburg port, the highest pCO_2 values (2074 µatm) were recorded, indicate strong CO_2 degassing. While further downstream, the pCO_2 decreased again (Table 2). In other European estuaries a similar pCO_2 pattern has been recorded (Frankignoulle et al., 1998). Lastly, taking into account the pO_2, which mirrored the pCO_2 evolution along the estuary, we could estimate respective sea to air (in case of CO_2) and air to sea (in case of O_2) fluxes (Fig. 4a).
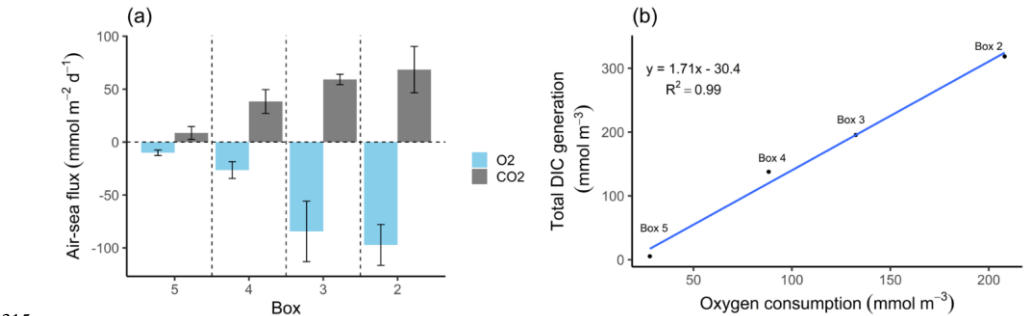
315
Figure 4. O_2 and CO_2 characteristics. (a) Air-sea fluxes (ASF) of oxygen (O_2) and carbon dioxide (CO_2) per box. The O_2 ASF were calculated from pO_2 and observed oxygen concentrations, and the CO_2 ASF were calculated from pCO_2 values and observed TA (Table 2). Values are shown with standard deviation represented as spatial variability (error bars). Positive values indicate outgassing, while negative values indicate a gas uptake into the water. The Hamburg port area is located in box 2, and the lower estuary in box 5. (b) Relationship

320 between metabolic DIC generation and O_2 consumption along the estuary in concentration (mmol m^{-3}). Please note the different parameters in the panels.

~~The highest metabolic DIC generation and O₂ consumption (Fig. 4a,b, Table 2) occurred in the port of Hamburg, where most of the CO₂ produced remained dissolved, with only a moderate amount being emitted to the atmosphere. The strong metabolic~~

Table 2. Average calculated gas values per box. O_2 concentration is the observed oxygen. O_2 consumption is the amount of oxygen consumed (i.e. AOU + oxygen uptake). Metabolic DIC gen. is the generated DIC. O_2 ASF is the oxygen, and CO_2 ASF is the carbon dioxide air-sea flux along the surface. Positive flux values indicate outgassing, while negative values indicate an absorption into the water. pCO₂ is the partial pressure of carbon dioxide, and corresponds to the CO_2 concentration in the water. The standard deviation ± sd as spatial variability
335 is given when possible. An uncertainty estimation including the uncertainties of the analytical measurements, the air-sea flux estimation, and the river discharge is given as (± absolute errors) by an error propagation (Methods).

Species	Unit	Box 1	Box 2	Box 3	Box 4	Box 5
Elbe stream km	km	607 - 619	619 - 639	639 - 666	666 - 693	693 - 710
O₂ concentration ± sd	mmol m⁻³	316 ± 10	193 ± 16	210 ± 30	264 ± 9	278 ± 2
O₂ consumption	mmol m⁻³	-	208 (± 15.7)	133 (± 30.3)	88 (± 21.3)	28 (± 20.7)
Metabolic DIC gen.	mmol m⁻³	-	319 (± 5.4)	196 (± 18.8)	138 (± 12.5)	6 (± 4.0)
O₂ ASF ± sd	mmol m⁻² d⁻¹	53 ± 12	-97 ± 19	-84 ± 28	-26 ± 8	-10 ± 3
CO₂ ASF ± sd	mmol m⁻² d⁻¹	2 ± 14	68 ± 22	59 ± 5	38 ± 11	9 ± 6
pCO₂ ± sd	µatm	465 ± 341	2074 ± 488	1833 ± 120	1554 ± 210	713 ± 208

The highest metabolic DIC generation and O_2 consumption (Fig. 4a,b, Table 2) occurred in the port of Hamburg, where most of the CO_2 produced remained dissolved, with only a moderate amount being emitted to the atmosphere. The strong metabolic
340 activity is also reflected by the high oxygen influx, driven by low oxygen conditions in the port of Hamburg (Table 2, see for example Amann et al. (2012) and Schöl et al. (2014)). In Figure 4b, the high slope of 1.71 of DIC and O_2 exceeds the ratio of 0.5 to 1 (e.g. Thomas (2002)), indicating anaerobic or particulate inorganic DIC sources. This therefore suggests that the remnants of the high metabolic activity in box 2 are transported further downstream, eventually approaching an equilibrium within the lower estuary (box 5, Fig. 4a,b). Accordingly, the observed metabolic values obtained for DIC (Fig. 5) and O₂
345 (AOU, Fig. 3) are to a large degree advected signals.

Using the mass balances, we calculated the net dissolved budgets of TA, DIC, and NO₃⁻, where only the net gains were represented but no indication of what processes were responsible for it. The highest metabolic gains of both TA and DIC were found in the Hamburg port area (box 2), identifying this area to have the highest metabolic activity (Fig. 5), almost an order of magnitude larger than that found in the downstream boxes. Accordingly, very high metabolic fluxes, i.e. area and time
350 normalized values, of TA (808 mmol m⁻² d⁻¹) and DIC (1164 mmol m⁻² d⁻¹) were obtained for the Hamburg port area (box 2)

(Fig. 5, Table 3). Downstream of the Hamburg port, values below 150 mmol m^{-2} d^{-1} and decreasing toward the North Sea were found, with negligible values in box 5. Similarly, the contribution of metabolically generated DIC is higher in the port area, than downstream, where CO_2 equilibration with the atmosphere gains (relative) importance. Compared to the metabolic gains, the air-sea flux (ASF) constitutes only a minor fraction of the metabolic fluxes (Fig. 5). The high release of DIC relative to TA

355 (Fig. 5) are in line with our above result of high pCO_2 in box 2 (Fig. 4a).

In contrast to TA and DIC, the metabolic NO_3^- fluxes have a similar magnitude along the estuary, with the highest fluxes (63 mmol m^{-2} d^{-1}) in the port of Hamburg, and lower fluxes (between 16 and 21 mmol m^{-2} d^{-1}) in the downstream parts of the estuary. Albeit, compared to TA and DIC, the relative difference between box 2 and the downstream boxes is much smaller for NO_3^- (Fig. 5).

360 For the entire Elbe Estuary, we estimated the total dissolved metabolic DIC and TA loads from all boxes released into the ~~Elbe Estuary in the~~ North Sea (excluding the air-sea fluxes). Our calculations yield annual metabolic loads of 5.6 Gmol yr^{-1} for TA and 6.5 Gmol yr^{-1} for DIC. In relation to the most recent data from 2017 (Pätsch and Lenhart, 2019), these metabolic loads represent 16 % of the overall DIC (39.6 Gmol DIC yr^{-1}) and 14 % of the overall TA (40.3 Gmol TA yr^{-1}) Elbe loads.

365
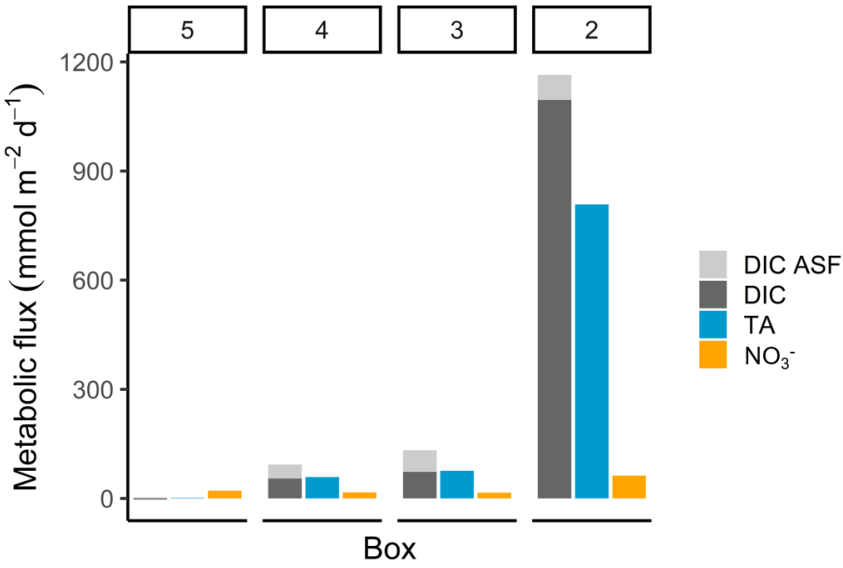
Figure 5. Metabolic fluxes of total alkalinity, dissolved inorganic carbon, and nitrate. The metabolic fluxes of TA (blue), DIC (dark grey) and NO_3^- (orange) in mmol m^{-2} d^{-1} are shown, with additionally visualizing the air-sea flux (ASF) contribution to DIC (light grey) to demonstrate the entire generation and their relative magnitude.

370 ~~We estimated the total dissolved metabolic DIC and TA loads from all boxes released into the Elbe Estuary in the North Sea (excluding the air-sea fluxes). Our calculations yield annual metabolic loads of 5.6 Gmol yr^{-1} for TA and 6.5 Gmol yr^{-1} for DIC. In relation to the most recent data from 2017 (Pätsch and Lenhart, 2019), these metabolic loads represent 16 % of the overall DIC (39.6 Gmol DIC yr^{-1}) and 14 % of the overall TA (40.3 Gmol TA yr^{-1}) Elbe loads.~~

3.3 Carbon based constraints on TA generation

375 In order to explain the net total alkalinity gains generated in the Elbe Estuary that were identified with the mass balances, we compared them to imported riverine particulate organic matter (POM) properties from samples taken simultaneously to our Elbe transect (Table 3). Natural variability, such as seasonality, may change the imports and lead to modified amounts of TA generation by the different processes.

Here, we used imported riverine particulate inorganic and organic carbon (PIC, POC) properties to attribute the TA gain fueled
380 by calcium carbonate ($CaCO_3$) dissolution and to estimate the remaining PIC amount that is transported downstream to identify a possible $CaCO_3$ deficit along the estuary.

We obtained TA generation from $CaCO_3$ dissolution referring to the metabolic, i.e. POM driven, DIC generation multiplied by the observed PIC:TC ratio of 0.29 ± 0.05 (average of entire estuary) of the imported POM. We assumed spontaneous, i.e. maximum dissolution of $CaCO_3$, which integrated over the estuary, can contribute up to 90 % of the TA generation and can
385 be considered as an upper bound. This result can be supported by the studies of Kempe (1982) and Francescangeli et al. (2021), who report undersaturated calcite saturation states (Ω) in the upper estuary and at their most fresh water station in the middle estuary.

Our estimate should be considered an upper bound, since other anaerobic metabolic processes must provide the remaining at least 10 % of the generated TA we observed. However, our data set does not allow us to directly identify or even quantify any
390 of these processes, nor does it allow us to exclude them.

In order to estimate the contribution of denitrification as a source for TA generation in the Elbe Estuary and to shed further light on the coupling between TA and nitrogen cycles, we related imported riverine particulate organic nitrogen (PON) to metabolically released NO_3^-.

Without NO_3^- generation by nitrification, we could explain TA generation by denitrification with around 9 % of the overall
395 metabolic TA gain. However, under consideration of both processes occurring in the estuary, we were unable to further attribute denitrification as the entire source for the TA generation in the Elbe Estuary. We identified a nitrogen deficit of riverine imported PON to fuel both NO_3^- generation (i.e. by nitrification) and TA generation (i.e. by denitrification) in boxes 4 and 5 (Table 3) that affect the balance of the entire estuary. This in turn means that lateral NO_3^- sources need to be inferred

to balance the nitrogen budget. Similarly, the fairly constant NO_3^- gain along the estuary (Fig. 5), but both decreasing O_2 consumption and DIC generation downstream (Figs. 4b, 5) imply a surplus of nitrate in the downstream part, thus a decoupling between carbon and nitrogen cycling.

To provide further evidence for lateral NO_3^- sources (Kendall et al., 2007;Middelburg and Nieuwenhuize, 2001;Sigman et al., 2001), we employed nitrate stable isotope ($\delta^{15}N$, $\delta^{18}O$) signatures. Similar to Dähnke et al. (2008), minimum $\delta^{15}N$ and $\delta^{18}O$ values were found in the section with maximum observed NO_3^- concentrations (box 5). The minima were lower than would be expected based on conservative mixing of North Sea and riverine end-members, as well as from nitrification processes during the 10-30 days downstream transport of waters (see for example Spieckermann et al. (2021)) (Fig. 3a). Nitrification preferentially releases lighter nitrate, depending on the sources for nitrification as evidenced by both decreasing $\delta^{15}N$ values in NO_3^- and increasing $\delta^{15}N$ values in SPM (Fig. 3a), but cannot explain the observed local minimum alone. The minimum in isotopic signature is in line with assumed delta values of the added nitrate (Eq. 2) of 7.1 ‰ for $\delta^{15}N-NO_3^-$ and -1.6 ‰ for $\delta^{18}O-NO_3^-$ (Table 4), which in turn points to an allochthones, lateral nitrate source. Such can be fueled by soil ammonium oxidation, manure and septic waste (Kendall et al., 2007), which can be identified as nitrogen sources with sufficiently light $\delta^{15}N$ and $\delta^{18}O$ characteristics. Although our study implies a lateral NO_3^- source, in contrast to earlier studies (Dähnke et al., 2008;Sanders et al., 2018), we cannot elucidate the corresponding source processes and regions in the context of this study.

Within the entire estuary, the spatial distributions of NO_3^- gain on one hand and the O_2 consumption and metabolic DIC generation on the other hand, show incoherent patterns. We found a decoupling of carbon, nitrogen and oxygen in the middle and lower estuary, with a fairly constant NO_3^- gain along the estuary (Fig. 5), but both decreasing O_2 consumption and DIC generation river downstream (Figs. 4b, 5). Thus, neither O_2 nor DIC reflect the NO_3^- gain, suggesting additional nitrate sources in the downstream fresh water part of the estuary.

Accordingly, estuarine ecosystems appear to be highly susceptible to nutrient management actions that affect the balance of the various metabolic processes that generate TA by controlling NO_3^- availability, as organic carbon and oxygen supply appear in excess or steady, respectively. One could speculate that the reduced organic carbon supply would reduce the importance of anaerobic processes in favor of a relative increase in aerobic respiration. On the other hand, a reduction in NO_3^- for a given organic carbon content would trigger other anaerobic processes (e.g iron or sulfate reduction) that have a higher TA gain per unit of carbon respired than does denitrification (Chen and Wang, 1999).

Table 3. Mass balance results and POM properties. The mass balance results are shown as metabolic generation (i.e. gains) in concentrations (mmol m^{-3}), in fluxes of total alkalinity (TA), dissolved inorganic carbon (DIC), and nitrate (NO_3^-), respectively (metabolic fluxes are also visualized in Fig. 5), and in kmol d^{-1}. The average carbon:nitrogen (C:N) and particulate inorganic carbon:total carbon (PIC:TC) ratios of suspended particulate matter (SPM) are given per box. The observed imported POC and particulate organic nitrogen (PON) values based on sampled filters in box 1, and the calculated transported values for PON in the other boxes (2-5) (sect. 2.3) are shown. Imported PIC for box 1 was calculated based on imported POC, and transported PIC values were calculated for the other boxes (2-5) (sect. 2.3). DIC fueled by PIC, and TA fueled by PIC give the amount of each that can be fueled of imported and transported PIC. DIC not fueled by PIC, and TA not fueled by PIC give the amount of each that is the remaining and not fueled of imported PIC or i.e. CaCO$_3$ dissolution.

The standard deviation ± sd as spatial variability is given when possible. An uncertainty estimation for analytical measurements, the air-sea flux estimation and the river discharge is given as (± absolute errors) by an error propagation (sect. 2.3). Imported POC, PIC and PON to the estuary was estimated using measured average POC (596 ± 52 µmol L^{-1}), and PON (91 ± 8 µmol L^{-1}) concentrations of SPM (47 ± 5 mg L^{-1}), all determined for box 1. PIC is here a synonym for $CaCO_3$ dissolution as source.

Species	Unit	Box 1	Box 2	Box 3	Box 4	Box 5
Metabolic TA gen.	mmol m^{-3}	-	221 (± 3.6)	112 (± 3.6)	87 (± 3.6)	1 (± 3.6)
Metabolic DIC gen.	mmol m^{-3}	-	319 (± 5.4)	196 (± 18.8)	138 (± 12.5)	6 (± 4.0)
Metabolic NO$_3^-$ gen.	mmol m^{-3}	-	17 (± 0.9)	23 (± 0.9)	24 (± 0.9)	20 (± 0.9)
Metabolic TA flux	mmol m^{-2} d^{-1}	-	808 (± 13.3)	76 (± 2.5)	59 (± 2.5)	1 (± 3.9)
Metabolic DIC flux	mmol m^{-2} d^{-1}	-	1164 (± 19.6)	132 (± 12.7)	93 (± 8.5)	6 (± 4.3)
Metabolic NO$_3^-$ flux	mmol m^{-2} d^{-1}	-	63 (± 3.3)	16 (± 0.6)	17 (± 0.6)	21 (± 1.0)
Av. C:N ± sd	-	6.6 ± 0.1	7.1 ± 1.1	7.9 ± 0.5	7.9 ± 0.4	7.5 ± 0.4
Av. PIC:TC ± sd	-	0.286 ± 0.25	0.192 ± 5.33	0.294 ± 0.62	0.314 ± 0.25	0.365 ± 0.33
Metabolic NO$_3^-$	kmol d^{-1}	-	625.3	857.5	893.5	723.0
Metabolic DIC	kmol d^{-1}	-	11644.3	7146.7	5036.9	196.2
Metabolic TA	kmol d^{-1}	-	8083.7	4090.6	3178.7	44.9
Imported POC	kmol d^{-1}	21788.9 (± 11.4)	-	-	-	-
Imported PON	kmol d^{-1}	3322.9 (± 0.2)	1219.7 (± 0.2)	422.7 (± 0.2)	-756.7 (± 0.2)	-646.5 (± 0.2)
Imported PIC	kmol d^{-1}	6318.8 (± 3.3)	5883.9 (± 3.3)	1738.8 (± 3.3)	-1182.6 (± 3.3)	-113.8 (± 3.3)
DIC fueled by PIC	kmol d^{-1}	-	3376.8 (± 196.7)	2072.5 (± 687.0)	1460.7 (± 457.2)	56.9 (± 147.7)
DIC not fueled by PIC	kmol d^{-1}	-	8267.4 (± 196.7)	5074.2 (± 687.0)	3576.2 (± 457.2)	139.3 (± 147.7)
TA fueled by PIC	kmol d^{-1}	-	6753.7 (± 196.7)	4145.1 (± 687.0)	2921.4 (± 457.2)	113.8 (± 147.7)
TA not fueled by PIC	kmol d^{-1}	-	1330.1 (± 237.4)	-54.5 (± 699.7)	257.3 (± 476.2)	-68.9 (± 198.7)

Table 4. Added nitrate values. The initial values and the changes of the nitrate concentration (µmol L^{-1}) and its associated stable isotopes (δ values in ‰) between Elbe stream km 609 and 705 are shown.

NO$_3^-$ [µmol L^{-1}]		NO$_3^-$ increase		δ^{15}N-NO$_3^-$ [‰]			δ^{18}O-NO$_3^-$ [‰]		
609	705	[µmol L^{-1}]	[%]	609	705	Added δ^{15}N-NO$_3^-$	609	705	Added δ^{18}O-NO$_3^-$
73.9	164.8	90.8	122.9	17.1	11.5	7.1	8.9	3.1	-1.6

3.4 Estuarine carbon release and estimated impact on coastal carbon storage

The impacts of anthropogenic and management activities on estuarine and coastal carbon cycling, as well as CO_2 uptake have frequently been discussed from an aerobic perspective, as for example by Borges and Gypens (2010) for the southern North Sea. Here we attempt to complement this perspective by considering anaerobic processes. We employed a biogeochemical simulation approach (Schwichtenberg et al., 2020) to estimate the impacts of estuarine metabolic TA gains on the carbon cycle

and CO_2 uptake capacity in the North Sea. We used this simulation approach to highlight the effect of changing DIC:TA ratios, e.g. due to anthropogenic induced changes, on the carbon storage in coastal oceans. Conceptually, the simulations reflect the relative balance between aerobic and anaerobic respiration of a given amount of organic carbon, such that any reduced
450   alkalinity scenario replies a preference for aerobic processes, and the increased alkalinity scenarios in turn imply a preference of anaerobic processes releasing a given amount of DIC. We applied four scenarios in which we changed the TA loads as input variable, and compared the resulting CO_2 uptake by the North Sea at three different distances from coast. For the first scenario, the reference run (i.e. normal condition), we used the full riverine TA and DIC load that correspond to a TA load of 100 %. For the second scenario, we reduced the TA load to 86 % reflecting the above contribution (14 %) of metabolic alkalinity to
455   the overall alkalinity release by the Elbe Estuary. For further comparisons, we ran scenarios with a reduced TA load to 50 % and an increased TA load to 150 %. We extrapolated these scenarios to 254 rivers that discharge into the North Sea. Especially the major rivers and estuaries are either associated with a major port (e.g. Antwerp, Rotterdam, London or Bremerhaven), or are generally characterized as a highly turbid and heavily used waterway (e.g. Ems) that, like the Elbe Estuary, provide ideal conditions for anaerobic metabolic pathways.
460   Under reference conditions (100 % TA), the open North Sea (> 200 km distance from the coastline) absorbs more atmospheric CO_2, with carbon transported in the deeper zones via the continental shelf pump (Thomas et al., 2004), than the coastal zones (100 km distance) (Fig. 6, absolute ASF indicated by bars). This spatial distribution is also visible in the scenarios with reduced TA loads. Assuming a remaining TA load of 50 % and 86 %, we modeled less CO_2 uptake due to reduced metabolic alkalinity generations.
465   Compared to the reduced TA scenarios, the increased TA scenario (150 %) also has higher CO_2 uptake within each distance, but in spatial distribution, higher CO_2 uptake in coastal areas than in the open North Sea. This indicates that in the 150 % scenario the open North Sea no longer represents the area of strongest CO_2 uptake.

The differences in CO_2 uptake in the North Sea (Fig. 6, difference ASF indicated by lines) between the scenarios with reduced TA (50 & 86 %) and the reference scenario (100 %) decreased with increasing distance from the coast. This change is also
470   reflected in the difference in CO_2 uptake between the scenario with increased TA load (150 %) and the reference scenario, where the difference in CO_2 uptake is higher in the coastal area than in the open ocean. This phenomenon can be partly explained by mixing, as the signal is the more diluted the further off shore. Furthermore, CO_2 equilibration continues as waters are transported offshore (e.g. Burt et al. (2014)), i.e. away from the TA source. The larger differences in CO_2 uptake in coastal areas suggest that the effects of TA input from metabolic processes in rivers are similar in magnitude to the simulated (Fig. 6)
475   and observed (Thomas et al., 2004) air-sea flux itself. Similar evidence has been presented by Burt et al. (2016), who report that benthic sediment release in the southern North Sea shapes, if not dominates, the seasonal variability of the TA system (see also Thomas et al. (2009)).
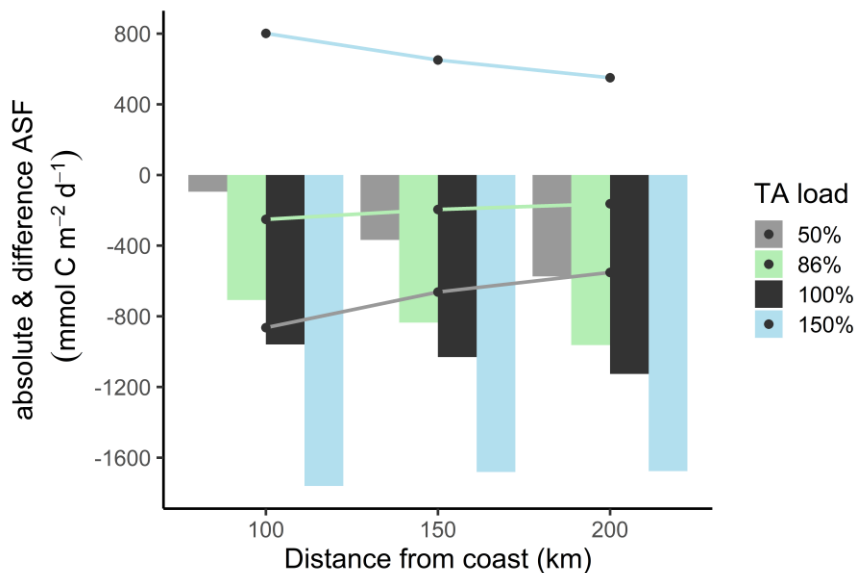
Figure 6. Biogeochemical CO₂ air-sea flux (ASF) simulations at distance from coast. The bars show the annual absolute CO_2 uptake in the water under reduced (50 %, grey) and (86 %, green), normal (100 %, black) and increased (150 %, blue) TA load. The lines visualize the CO_2 uptake difference between the scenarios 50, 86, 150 %, and the reference scenario (100 %).

Next to CO_2 air-sea fluxes, the metabolic TA release from the Hamburg port area could also affect calcifying organisms such as foraminifera that occur in the lower Elbe Estuary. In a recent study, Francescangeli et al. (2021) observed the change of calcite saturation state (Ω_{Ca}) from under- to supersaturation around Elbe km 685 (approx.). Without the respective TA generation, the supersaturated range and thus, the habitat of the foraminifera, would clearly be further downstream, if not restricted to the North Sea. For example, at their most saline station (Francescangeli et al. (2021), see their Fig. 2f), corresponding to Elbe stream km 730 in our study, the observed Ω_{Ca} is ~ 3.3, whereas it would be strongly undersaturated (Ω_{Ca} ~ 0.2) without benthic TA release.

4 Conclusions

We observed clear regional differences in the biogeochemistry of the Elbe Estuary. While conservative mixing prevails in the salinity gradient of the lower estuary, metabolic processes dominate the upper, fresh water part within the port of Hamburg.

We observed a strong increase of several hundred µmol kg^{-1} of TA and DIC in the Hamburg port (Fig. 3) with diminishing vanishing values downstream, and calculated an annual metabolic TA load of about 14 % of the total TA runoff from the Elbe River to the coastal ocean.

Mass balances suggest that up to 90 % of the generated TA of the entire estuary could be fueled by imported PIC, i.e. through $CaCO_3$ dissolution. And that, the remaining 10 % of the generated TA may be due to anaerobic metabolic processes such as denitrification, iron, manganese, or sulfate reduction. Nevertheless, the uncertainty of natural variabilities such as seasonality or extreme weather (e.g. dry or rain events), may exert control over relative and absolute occurrence of above processes. However, the interplay of the various metabolic processes governs both the release of reduced products and the carbonate system properties in the estuary. For example, the former controls the balance of released gases such as N_2, N_2O and H_2S, which in turn can have negative effects on the entire estuarine biodiversity, leading to losses in reproduction and habitats of e.g. local fish species (Breitburg et al., 2009;Breitburg, 2002;Janas and Szaniawska, 1996;Wu, 2009). The carbonate system properties regulate the habitable range for example for benthic foraminifera (Francescangeli et al., 2021). We show that the metabolic TA release increases the capacity and CO_2 absorption in the German Bight. Compared to the open ocean, the coastal ocean would act as a stronger CO_2 sink with increased TA loads. We postulate that this result may be transferable to other global rivers or estuarine systems, particularly those with large port facilities, and that it could have tangible implications for the ocean's CO_2 uptake capacity on a global scale.

Data availability

The datasets generated during and/or analyzed during the current study are either presented in the study, and are in preparation to be released in accordance with the rules of the funding agency.

Author contributions

MN, KD, and HT designed the study. MN did the sampling, sample measurements and analyses, data interpretation and evaluation, and prepared the manuscript. JP did the biogeochemical simulation by using the 3D-ECOHAM model. GS performed stable isotope measurements, data analysis and interpretation, and added to the method description. KD, TS, JP, JVB, and HT provided scientific and editorial recommendations. MN wrote the manuscript with input from all co-authors.

Competing interests

The authors declare that they have no conflict of interest.

Acknowledgement

520 This research has been funded by the German Academic Exchange Service (DAAD, project: MOPGA-GRI, grant no. 57429828), which received funds from the German Federal Ministry of Education and Research (BMBF).

We thank our crew of the RV *Ludwig Prandtl* for their helping hands during the sampling campaign. Thanks to Leon Schmidt for measuring the nutrients, our intern Jeannette Hansen for supporting us with the box model calculation, Linda Baldewein for supporting us with the Elbe River kilometer calculation, the working group of biogeochemistry at the Institute of Geology,

525 University Hamburg for measuring the filters, and Yoana Voynova for providing the FerryBox data. The oxygen calibration samples were collected by Götz Flöser, analyzed by Tanja Pieplow, and processed by Yoana Voynova. Martina Gehrung did the FerryBox preparation (optode specific). We thank Chantal Mears for thoroughly proofreading. We thank the Editor Perran Cook, and two anonymous reviewers whose helpful comments greatly improved the manuscript.

References

530 Abril, G., Nogueira, M., Etcheber, H., Cabeçadas, G., Lemaire, E., and Brogueira, M.: Behaviour of organic carbon in nine contrasting European estuaries, Estuarine, coastal and shelf science, 54, 241-262, 2002.

Amann, T., Weiss, A., and Hartmann, J.: Carbon dynamics in the freshwater part of the Elbe estuary, Germany: Implications of improving water quality, Estuarine, Coastal and Shelf Science, 107, 112-121, 2012.

Backhaus, J. O.: A three-dimensional model for the simulation of shelf sea dynamics, Deutsche Hydrografische Zeitschrift, 38, 165-187, 535 1985.

Backhaus, J. O., and Hainbucher, D.: A finite difference general circulation model for shelf seas and its application to low frequency variability on the North European Shelf, in: Elsevier oceanography series, Elsevier, 221-244, 1987.

Borges, A., Schiettecatte, L.-S., Abril, G., Delille, B., and Gazeau, F.: Carbon dioxide in European coastal waters, Estuarine, Coastal and Shelf Science, 70, 375-387, 2006.

540 Borges, A. V., and Gypens, N.: Carbonate chemistry in the coastal zone responds more strongly to eutrophication than ocean acidification, Limnology and Oceanography, 55, 346-353, 2010.

Breitburg, D.: Effects of hypoxia, and the balance between hypoxia and enrichment, on coastal fishes and fisheries, Estuaries, 25, 767-781, 2002.

Breitburg, D. L., Craig, J. K., Fulford, R. S., Rose, K. A., Boynton, W. R., Brady, D. C., Ciotti, B. J., Diaz, R., Friedland, K., and Hagy, J.: 545 Nutrient enrichment and fisheries exploitation: interactive effects on estuarine living resources and their management, Hydrobiologia, 629, 31-47, 2009.

Brewer, P. G., and Goldman, J. C.: Alkalinity changes generated by phytoplankton growth 1, Limnology and Oceanography, 21, 108-117, 1976.

Burt, W., Thomas, H., Pätsch, J., Omar, A., Schrum, C., Daewel, U., Brenner, H., and de Baar, H.: Radium isotopes as a tracer of sediment-550 water column exchange in the North Sea, Global Biogeochemical Cycles, 28, 786-804, 2014.

Burt, W., Thomas, H., Hagens, M., Pätsch, J., Clargo, N., Salt, L., Winde, V., and Böttcher, M.: Carbon sources in the North Sea evaluated by means of radium and stable carbon isotope tracers, Limnology and Oceanography, 61, 666-683, 2016.

Cai, W. J., and Wang, Y.: The chemistry, fluxes, and sources of carbon dioxide in the estuarine waters of the Satilla and Altamaha Rivers, Georgia, Limnology and Oceanography, 43, 657-668, 1998.

555 Casciotti, K. L., Sigman, D. M., Hastings, M. G., Böhlke, J., and Hilkert, A.: Measurement of the oxygen isotopic composition of nitrate in seawater and freshwater using the denitrifier method, Analytical chemistry, 74, 4905-4912, 2002.

Chen, C. T. A., and Wang, S. L.: Carbon, alkalinity and nutrient budgets on the East China Sea continental shelf, Journal of Geophysical Research: Oceans, 104, 20675-20686, 1999.

Cysewski, M., Seemann, J., and Horstmann, J.: Artifacts or Nature? Data Processing and Interpretation of 3D Current Fields Recorded with 560 Vessel Mounted Acoustic Doppler Current Profiler in Different Regions and Conditions, 2018 OCEANS-MTS/IEEE Kobe Techno-Oceans (OTO), 2018, 1-5,

Dähnke, K., Bahlmann, E., and Emeis, K.: A nitrate sink in estuaries? An assessment by means of stable nitrate isotopes in the Elbe estuary, Limnology and Oceanography, 53, 1504-1511, 2008.

De Jonge, V. N., Boynton, W., D'Elia, C. F., Elmgren, R., and Welsh, R.: Responses to developments in eutrophication in four different North Atlantic estuarine systems, OLSEN & OLSEN, FREDENSBORG, DENMARK., 179-196, 1994.

Dlugokencky, E., and Tans, P.: Trends in atmospheric carbon dioxide. National Oceanic and Atmospheric Administration, Earth System Research Laboratory (NOAA/ESRL), 2021.

DWD, Deutscher Wetter Dienst (DWD), Climate Data Center (CDC), https://www.dwd.de/DE/klimaumwelt/cdc/cdc_node.html, 2020.

FGG, Flussgebietsgemeinschaft (FGG) Elbe, https://www.elbe-datenportal.de/FisFggElbe/content/auswertung/UntersuchungsbereichHydro_start_x.action,, 2021.

Francescangeli, F., Milker, Y., Bunzel, D., Thomas, H., Norbisrath, M., Schönfeld, J., and Schmiedl, G.: Recent benthic foraminiferal distribution in the Elbe Estuary (North Sea, Germany): A response to environmental stressors, Estuarine, Coastal and Shelf Science, 251, 107198, 2021.

Frankignoulle, M., Bourge, I., and Wollast, R.: Atmospheric CO2 fluxes in a highly polluted estuary (the Scheldt), Limnology and Oceanography, 41, 365-369, 1996.

Frankignoulle, M., Abril, G., Borges, A., Bourge, I., Canon, C., Delille, B., Libert, E., and Théate, J.-M.: Carbon dioxide emission from European estuaries, Science, 282, 434-436, 1998.

Gaye, B., Lahajnar, N., Harms, N., Paul, S. A. L., Rixen, T., and Emeis, K.-C.: What can we learn from amino acids about oceanic organic matter cycling and degradation?, Biogeosciences, 19, 807-830, 2022.

Gilbert, D., Sundby, B., Gobeil, C., Mucci, A., and Tremblay, G. H.: A seventy-two-year record of diminishing deep-water oxygen in the St. Lawrence estuary: The northwest Atlantic connection, Limnology and oceanography, 50, 1654-1666, 2005.

Granger, J., and Sigman, D. M.: Removal of nitrite with sulfamic acid for nitrate N and O isotope analysis with the denitrifier method, Rapid Communications in Mass Spectrometry: An International Journal Devoted to the Rapid Dissemination of Up-to-the-Minute Research in Mass Spectrometry, 23, 3753-3762, 2009.

Große, F., Greenwood, N., Kreus, M., Lenhart, H.-J., Machoczek, D., Pätsch, J., Salt, L., and Thomas, H.: Looking beyond stratification: a model-based analysis of the biological drivers of oxygen deficiency in the North Sea, Biogeosciences, 13, 2511-2535, 2016.

Große, F., Kreus, M., Lenhart, H.-J., Pätsch, J., and Pohlmann, T.: A novel modeling approach to quantify the influence of nitrogen inputs on the oxygen dynamics of the North Sea, Frontiers in Marine Science, 4, 383, 2017.

Hansen, H., and Koroleff, F.: Determination of nutrients. Methods of Seawater Analysis: Third, Completely Revised and Extended Edition. Weinheim, Germany: Wiley-VCH Verlag GmbH, 2007.

Hardenbicker, P., Weitere, M., Ritz, S., Schöll, F., and Fischer, H.: Longitudinal plankton dynamics in the rivers Rhine and Elbe, River Research and Applications, 32, 1264-1278, 2016.

Hersbach, H., Bell, B., Berrisford, P., Hirahara, S., Horányi, A., Muñoz-Sabater, J., Nicolas, J., Peubey, C., Radu, R., and Schepers, D.: The ERA5 global reanalysis, Quarterly Journal of the Royal Meteorological Society, 146, 1999-2049, 2020.

Howarth, R., Chan, F., Conley, D. J., Garnier, J., Doney, S. C., Marino, R., and Billen, G.: Coupled biogeochemical cycles: eutrophication and hypoxia in temperate estuaries and coastal marine ecosystems, Frontiers in Ecology and the Environment, 9, 18-26, 2011.

Howarth, R. W., Billen, G., Swaney, D., Townsend, A., Jaworski, N., Lajtha, K., Downing, J. A., Elmgren, R., Caraco, N., and Jordan, T.: Regional nitrogen budgets and riverine N & P fluxes for the drainages to the North Atlantic Ocean: Natural and human influences, in: Nitrogen cycling in the North Atlantic Ocean and its watersheds, Springer, 75-139, 1996.

Hu, X., and Cai, W. J.: An assessment of ocean margin anaerobic processes on oceanic alkalinity budget, Global Biogeochemical Cycles, 25, 2011.

Janas, U., and Szaniawska, A.: The influence of hydrogen sulphide on macrofaunal biodiversity in the Gulf of Gdansk, Oceanologia, 38, 127-142, 1996.

Kempe, S.: Valdivia cruise, October 1981: carbonate equilibria in the estuaries of Elbe, Weser, Ems and in the Southern German Bight, Transport of carbon and minerals in major world rivers. Univ. Hamburg, 52, 719-742, 1982.

Kendall, C., Elliott, E. M., and Wankel, S. D.: Tracing anthropogenic inputs of nitrogen to ecosystems, Stable isotopes in ecology and environmental science, 2, 375-449, 2007.

Kerner, M.: Effects of deepening the Elbe Estuary on sediment regime and water quality, Estuarine, coastal and shelf science, 75, 492-500, 2007.

Kérouel, R., and Aminot, A.: Fluorometric determination of ammonia in sea and estuarine waters by direct segmented flow analysis, Marine Chemistry, 57, 265-275, 1997.

Léonard, J., Mietton, M., Najib, H., and Gourbesville, P.: Rating curve modelling with Manning's equation to manage instability and improve extrapolation, Hydrological sciences journal, 45, 739-750, 2000.

Lewis, E., and Wallace, D.: Program developed for CO2 system calculations, Environmental System Science Data Infrastructure for a Virtual Ecosystem, 1998.

Lorkowski, I., Pätsch, J., Moll, A., and Kühn, W.: Interannual variability of carbon fluxes in the North Sea from 1970 to 2006–Competing effects of abiotic and biotic drivers on the gas-exchange of CO2, Estuarine, Coastal and Shelf Science, 100, 38-57, 2012.

Middelburg, J., and Nieuwenhuize, J.: Nitrogen isotope tracing of dissolved inorganic nitrogen behaviour in tidal estuaries, Estuarine, Coastal and Shelf Science, 53, 385-391, 2001.

620 Millero, F. J.: The thermodynamics of the carbonate system in seawater, Geochimica et Cosmochimica Acta, 43, 1651-1661, 1979.

Mucci, A., Starr, M., Gilbert, D., and Sundby, B.: Acidification of lower St. Lawrence Estuary bottom waters, Atmosphere-Ocean, 49, 206-218, 2011.

Nixon, S. W.: Coastal marine eutrophication: a definition, social causes, and future concerns, Ophelia, 41, 199-219, 1995.

Pätsch, J., and Kühn, W.: Nitrogen and carbon cycling in the North Sea and exchange with the North Atlantic—a model study. Part I.
625 Nitrogen budget and fluxes, Continental Shelf Research, 28, 767-787, 2008.

Pätsch, J., and Lenhart, H.: Daily Loads of Nutrients, Total Alkalinity, Dissolved Inorganic Carbon and Dissolved Organic Carbon of the European Continental Rivers for the Years 1977 – 2017, DATA RIVER, Universität Hamburg, 2019.

Pein, J., Eisele, A., Sanders, T., Daewel, U., Stanev, E. V., Van Beusekom, J. E., Staneva, J., and Schrum, C.: Seasonal Stratification and Biogeochemical Turnover in the Freshwater Reach of a Partially Mixed Dredged Estuary, Frontiers in Marine Science, 8, 623714, 2021.

Petersen, W., Schroeder, F., and Bockelmann, F.-D.: FerryBox-Application of continuous water quality observations along transects in the
630 North Sea, Ocean Dynamics, 61, 1541-1554, 2011.

Pohlmann, T.: Predicting the thermocline in a circulation model of the North Sea—Part I: model description, calibration and verification, Continental Shelf Research, 16, 131-146, 1996.

Rabalais, N. N., Turner, R. E., and Wiseman Jr, W. J.: Hypoxia in the Gulf of Mexico, Journal of environmental quality, 30, 320-329, 2001.

Rabalais, N. N., Turner, R. E., and Wiseman Jr, W. J.: Gulf of Mexico hypoxia, aka" The dead zone", Annual Review of ecology and
635 Systematics, 235-263, 2002.

Sanders, T., Schöl, A., and Dähnke, K.: Hot spots of nitrification in the Elbe estuary and their impact on nitrate regeneration, Estuaries and coasts, 41, 128-138, 2018.

Schöl, A., Hein, B., Wyrwa, J., and Kirchesch, V.: Modelling water quality in the Elbe and its estuary–Large Scale and Long Term
640 Applications with Focus on the Oxygen Budget of the Estuary, Die Küste, 81 Modelling, 203-232, 2014.

Schwichtenberg, F., Pätsch, J., Böttcher, M. E., Thomas, H., Winde, V., and Emeis, K.-C.: The impact of intertidal areas on the carbonate system of the southern North Sea, Biogeosciences, 17, 4223-4245, 2020.

Seitzinger, S. P.: Denitrification in freshwater and coastal marine ecosystems: ecological and geochemical significance, Limnology and oceanography, 33, 702-724, 1988.

645 Shadwick, E., Thomas, H., Gratton, Y., Leong, D., Moore, S., Papakyriakou, T., and Prowe, A.: Export of Pacific carbon through the Arctic Archipelago to the North Atlantic, Continental Shelf Research, 31, 806-816, 2011.

Sigman, D. M., Casciotti, K. L., Andreani, M., Barford, C., Galanter, M., and Böhlke, J.: A bacterial method for the nitrogen isotopic analysis of nitrate in seawater and freshwater, Analytical chemistry, 73, 4145-4153, 2001.

Smith, S., and Hollibaugh, J.: Coastal metabolism and the oceanic organic carbon balance, Reviews of Geophysics, 31, 75-89, 1993.

650 Spieckermann, M., Gröngröft, A., Karrasch, M., Neumann, A., and Eschenbach, A.: Oxygen Consumption of Resuspended Sediments of the Upper Elbe Estuary: Process Identification and Prognosis, Aquatic Geochemistry, 1-25, 2021.

Thomas, H.: Remineralization ratios of carbon, nutrients, and oxygen in the North Atlantic Ocean: A field databased assessment, Global Biogeochemical Cycles, 16, 24-21-24-12, 2002.

Thomas, H., Bozec, Y., Elkalay, K., and De Baar, H. J.: Enhanced open ocean storage of CO2 from shelf sea pumping, Science, 304, 1005-
655 1008, 2004.

Thomas, H., Schiettecatte, L.-S., Suykens, K., Koné, Y., Shadwick, E., Prowe, A. F., Bozec, Y., de Baar, H. J., and Borges, A.: Enhanced ocean carbon storage from anaerobic alkalinity generation in coastal sediments, Biogeosciences, 6, 267-274, 2009.

Van Beusekom, J. E., Carstensen, J., Dolch, T., Grage, A., Hofmeister, R., Lenhart, H., Kerimoglu, O., Kolbe, K., Pätsch, J., and Rick, J.: Wadden Sea Eutrophication: long-term trends and regional differences, Frontiers in Marine Science, 370, 2019.

660 Wanninkhof, R.: Relationship between wind speed and gas exchange over the ocean revisited, Limnology and Oceanography: Methods, 12, 351-362, 2014.

Watson, A. J., Schuster, U., Bakker, D. C., Bates, N. R., Corbière, A., González-Dávila, M., Friedrich, T., Hauck, J., Heinze, C., and Johannessen, T.: Tracking the variable North Atlantic sink for atmospheric CO2, Science, 326, 1391-1393, 2009.

Wolf-Gladrow, D. A., Zeebe, R. E., Klaas, C., Körtzinger, A., and Dickson, A. G.: Total alkalinity: The explicit conservative expression and
665 its application to biogeochemical processes, Marine Chemistry, 106, 287-300, 2007.

Wu, R. S.: Effects of hypoxia on fish reproduction and development, in: Fish physiology, Elsevier, 79-141, 2009.